J Mar Sci Technol (2011) 16:143–156
DOI 10.1007/s00773-011-0119-0

ORIGINAL ARTICLE

Multi-fidelity optimization of a high-speed foil-assisted semi-planing catamaran for low wake

Manivannan Kandasamy · Daniele Peri · Seng Keat Ooi · Pablo Carrica · Frederick Stern · Emilio F. Campana · Philip Osborne · Jessica Cote · Neil Macdonald · Nic de Waal

Received: 24 September 2009 / Accepted: 17 February 2011 / Published online: 13 April 2011

Abstract The wakes of high-speed passenger-only ferries that operated through Rich Passage, on the Seattle-Bremerton ferry route, caused beach erosion and damage to habitat. A task was initiated to design a low-wake high-speed vessel using multi-fidelity CFD based design optimization by using low-fidelity potential flow solvers for initial global design optimization and by using URANS solvers for high-fidelity tuning of the optimized design. This simulation based design process involved a close collaboration between ship designers, and hydrodynamics and CFD specialists, whose collective expertise guided the evolution of the design based on both hydrodynamic and structural aspects. The initial hull shape optimization using potential flow code was carried out by blending three different initial concepts provided by the designers. Subsequently, URANS was used to evaluate the potential flow optimized hull and to further optimize the hull configuration parameters, namely, the centre-of-gravity, demihull spacing, foil location, foil angle and slenderness ratio at different displacement conditions. The URANS based configuration optimization also took into account the far field wakes' energy spectrum with an objective of reducing the energetic, low frequency far field wakes which are associated with beach flattening on the mixed sand and gravel beaches. Calculation of the far field wake using URANS would require an unfeasibly large domain size; therefore, a Havelock code with a source distribution matching the URANS calculated near field wave elevation was used to propagate the wakes into the far field. The end result of the optimization was a design with significantly reduced far field wake, which is currently being built for experimental testing.

Keywords Optimization · Foil assisted catamaran · High-speed · Far field wakes · URANS · Havelock sources

M. Kandasamy · S. K. Ooi · P. Carrica · F. Stern (✉)
University of Iowa, Iowa City, IA, USA
e-mail: frederick-stern@uiowa.edu

D. Peri · E. F. Campana
INSEAN, Rome, Italy

P. Osborne · J. Cote
Golder Associates Inc., 18300 NE Union Hill Road, Suite 200, Redmond, WA 98052, USA

N. Macdonald
Coldwater Consulting, Gloucester, ON, Canada

N. de Waal
Technicraft Ltd., Birkenhead, Auckland, New Zealand

1 Introduction

Water-jet propelled catamarans operating at speeds between 34 and 37 knots through the Rich Passage caused beach erosion, leading to their suspension. Shore impact studies with a 150-passenger foil-assisted catamaran (FAC), named SPIRIT, and subsequent integrated impact assessment modeling, indicated that the FAC vessel design shows considerable promise as a low-impact alternative. Vessel design considerations and measurements from vessel trials suggest that further improvements in wakes could be achieved with hull design optimization.

The objective of the current project was to design a passenger-only fast ferry capable of high speed, but with a lower wake based on the existing SPIRIT design. A CFD based design was carried out to meet the requirements for speed and wake. Low fidelity potential flow (PF) based multi-objective optimization was carried out during the initial design stages

[1] using three different base designs provided by the ship designers. A large design space was explored to find the optimum design for both speed and low wake over the design speed range. Starting from the hull lines of SPIRIT, a new design (hereafter referred to as RV2), meeting the requirements of the designer, was finally obtained, and a first investigation into the effect of a shape variation of the hull, the foils and of their mutual position was performed. Subsequent investigation involved the complete redesign of the bow and of the foil by using a morphing technique: three base designs were produced by Teknicraft Design Ltd., on the base of the indications coming from the results of the sensitivity study. The INSEAN SBD framework was then applied to solve the constrained multiobjective optimization problem. A set of optimal configurations with respect to three different criteria was finally derived and the final design was eventually identified. Finally, a sensitivity analysis around the optimal shape was produced in order to understand the hydrodynamic qualities of the selected geometry, and to give practical, useful indications to the designers.

Building on the results of the PF optimization, high fidelity URANS was used in the later stages of the design to arrive at a concept design deemed trustworthy for building and experimental testing. The URANS based design explored effects of ship waterline length (LWL), displacement, longitudinal centre of gravity (LCG), foil angle, foil position, distance between demihull centrelines (S_C), and demihull slenderness ratio (DSR = LWL/demihull waterline beam-BWL). Close collaboration with ship designers was key in this part of the design process as the constraints on the size and shape were dictated by parameters such as cost, passenger seating, available commercial engines compliant with emission regulations, and size/shape of available water jet propulsion at different displacements which evolved with the evolution of the design. Simulations were conducted at model scale and the results were extrapolated to full scale. Calculation of the far field wake using URANS would require an unfeasibly large domain, so a Havelock code with a source distribution matching the URANS calculated near field wave elevation was used to propagate the wakes to the far field. The PF code, URANS code and the extrapolation methods used in the design process were validated using field data from SPIRIT and 1060 [2].

Variable fidelity optimization has been successfully used previously on a SWATH type displacement ship where PF codes explored a wide design space, and URANS was used in the final design optimization using genetic algorithms to explore a limited design space [3]. However, for the present case, dealing with a semi-planing FAC with many more design variables and a much bigger solution space, probabilistic global optimization schemes like genetic algorithms were not feasible for URANS due to prohibitively large computational expense. In addition, the far field extrapolation method using the Havelock sources could not be easily automated for global optimization because different cases required different positioning of the sources and sinks to get a near field match, requiring individual treatment. Hence, the sensitivity of each design parameter was studied systematically for the URANS based optimization, to have better understanding of the effects of the individual parameters on the flow physics. Since the solution space is too large to be thoroughly explored, the direction of the systematic search method relied heavily on the expertise of the designers for guidance.

The remainder of the paper is structured as follows: The next section provides the ship designer's initial concept design, followed by sections devoted to the computational method used, details of the methodology, results from the optimization, and our conclusions.

2 Ship designer's initial conceptual designs

The design of a vessel hull needs to balance specific requirements in the optimum way. The first requirement for this vessel is to have a wake signature compliant with a newly developed wake criterion as described in [4]. Secondly, the vessel needs to be able to maintain a cruise speed of 35 knots. The distance between the ports is 13.5 nm, and a crossing time of 30 min is required to meet the service schedule. Considering that 3–5 min are spent at either end of the route at very low speed whilst approaching the terminals, the average speed to traverse the remaining 13 nm is 35 knots. Further important requirements include low fuel consumption, capacity of up to 150 passengers, good seakeeping to ensure a comfortable ride for passengers in all weather conditions, a cost on the same order as conventional high speed ferries which do not meet the requirements, and compliance with all US Coastguard requirements for a Subchapter T commercial vessel. Considering the requirements for this application, it is clear that there are conflicting criteria in terms of hull design. For instance, a hull that would produce a low wake at high speed with low resistance would not normally be a hull with good seakeeping in adverse sea conditions. The designer created three different hull shapes for the initial potential flow optimization [1]. The designs were named RV2A, RV2B, and RV2C.

2.1 RV2B

This hull is based on a shape which Teknicraft Design has developed over a period of 10 years, and of which approximately one hundred prototypes of various sizes are in service. The hull is an asymmetrical catamaran configuration shaped for optimum seakeeping. The outboard deadrise is round bilge shaped, which is the most effective shape to

reduce vertical acceleration, whilst maintaining load carrying ability. The inboard shape of the demi-hull is vertical, with pronounced horizontal chines. Vertical sides further enhance seakeeping characteristics and allow the clear tunnel area between the demi-hulls to be larger than normal. The large clear area has the effect that approaching waves, in particular wind generated waves with short wavelength, can pass through the tunnel without creating so-called tunnel slap, the phenomenon that occurs when green water hits the bridging structure and causes uncomfortable noise and vertical acceleration. The hull incorporates various features to reduce resistance without compromising seakindliness. The pronounced chines deflect green water from the hull at high speed (Fr (length) >1.0), which reduces the wetted area. A hydrofoil is designed to fit between the demi-hulls at approximately the level of the keels. As a practical consideration of vulnerability, the hydrofoil is not mounted any deeper. The lifting characteristic of the foil is designed to support a significant portion of the overall displacement of the vessel at design speed, however it is intentionally designed such that the demi-hulls still carry adequate displacement to ensure good seakeeping in rough sea conditions. The effect of the foil is to reduce the draft of the hull, and therefore reduce the wetted area at design speed. The hydrofoil does add resistance to the hull, however the net reduction in overall resistance due to the reduced wetted area is significant, and can be up to 35% in calm water compared to the resistance of the hull without a hydrofoil.

Previous wake studies, including [4], has proven this hullshape to have low wake pattern characteristics compared to conventional catamaran vessels, and the design therefore has good potential as a base for developing a hull which would exhibit all the required characteristics.

2.2 RV2A

This hullshape is similar to RV2B described above, but with certain differences to reduce wake energy. The inboard lower edge of the demi-hull is significantly rounded instead of squared. The squareness of RV2B assists in reducing resistance by creating a planing surface, as well as promoting clean flow around the tip of the foil, however it also generates a high pressure wave which would be detrimental to low wake pattern. The rounded edge would compromise low resistance in favour of low wake. The bow is finer and the stem rake steeper. The effect is reduced wave making tendency as well as a longer LWL with increased DSR.

2.3 RV2C

This is a symmetrical hull with low deadrise and rounded knuckles. A fine entry bow is designed to further increase LWL and DSR. The design has relatively low planing resistance due its large planing surfaces, but increased interference between the demi-hulls is expected to have a negative effect on wake pattern. To ensure that the hull-shapes are compared accurately, the hull length and beam, displacement, and static trim are kept constant for all three shapes.

3 Computational methods

3.1 Viscous solver

CFDSHIP-Iowa is a general purpose URANS/DES solver developed at IIHR over the last 15 years for ship hydrodynamics applications. For the current simulations, URANS with the blended $k-\omega/k-\varepsilon$ turbulence model was used. The free surface location is predicted by a single phase level set method. A second order upwind scheme is used to discretize the convective terms of the momentum equations for URANS. A pressure-implicit split-operator (PISO) algorithm is used to enforce mass conservation on the collocated grids. The pressure Poisson equation is solved using the PETSc toolkit [5]. All the other systems are solved using an alternating direction implicit (ADI) method. An MPI-based domain decomposition approach is used, where each decomposed block is mapped to one processor. The software SUGGAR [6] runs as a separate process from the flow solver to compute interpolation coefficients for the overset grids; it communicates with a motion controller (6DOF) within CFDSHIP-Iowa at every timestep. The software USURP [7] is used to compute area and forces on the surface overlap regions. For the thrust predictions, the ship is initially static on calm water and then allowed to pitch and heave under a constant inlet fluid velocity until a steady state is reached. Figure 1 shows the simulation domain and the overset grids used. The foil was modeled both attached to the hull and detached from the hull, as shown in Fig. 2. The detached foil was used for ease of changing foil angle and position during initial sensitivity studies. Due to the numerous foil angle/position configurations to be explored, initially the foil was detached from the hull to enable easier changes in the angle/position and was used to get general trends. However, the water escaping the gap between the foil and the hull created a loss of lift in the simulation results resulting in larger wetted surface area and hence an increase in resistance. In the later stages, once the foil position/angle trends were gathered, the foil was modeled attached to the hull to obtain more accurate results. A 5-million-point grid was used for all the calculations, based on a grid verification study done on ship-1060.

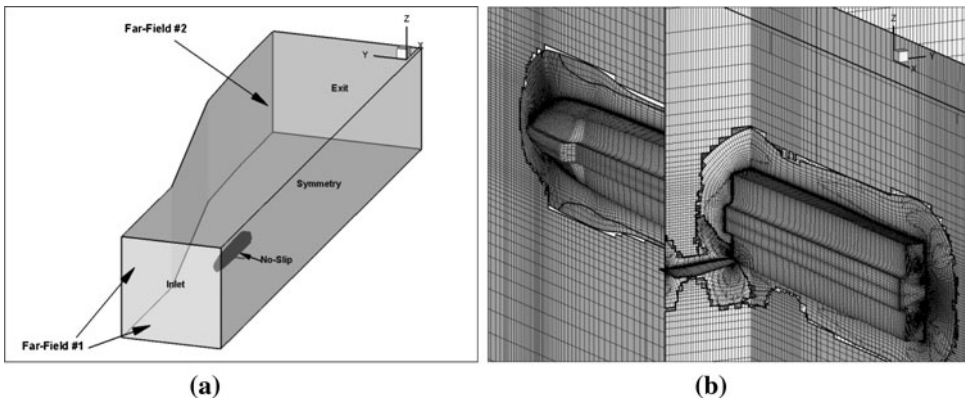

Fig. 1 **a** Extent of domain and boundary conditions and **b** overset grids for simulations that were carried out

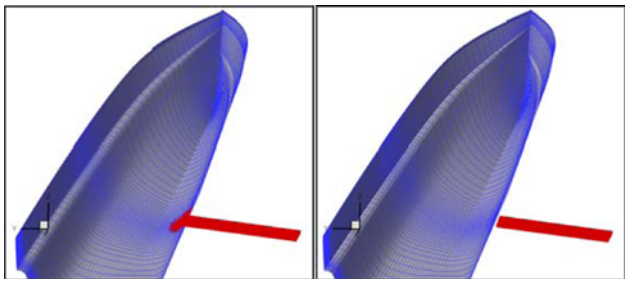

Fig. 2 Different treatments for foil modeling

3.2 Potential flow solver

WARP potential solver [8] is a classical boundary element method (BEM) type solver. Rankine sources, together with vortex rings, are arranged on the hull geometry and on a portion of the free surface around the ship. Desingularized panels are adopted on the free surface. Derivatives of the velocity potential are obtained analytically. Simulations are not affected by the scale, since the viscous terms are not directly considered during the solution, and an accurate estimate of the wave resistance is obtained by pressure integration or by wave cut analysis. The estimated resistance is represented by the wave resistance plus a frictional contribution obtained by means of a locally adapted friction line. The hull position is obtained by the equilibrium of the forces on the hull plus the thrust of the waterjet. Around 3000 panels have been used to discretize the hull surface, and 3000 panels were used on the free surface.

4 Overall methodology

The overall optimization process is described below.

1. Initial 3 RV designs (RV-2A, RV-2B, and R-2C) and 3 foils (F1, F2 and F3) were provided by designer based on PF shape sensitivity studies on SPIRIT;
2. Potential flow hull shape optimization was performed by an evolutionary optimization algorithm [9], morphing the initial designs;
3. URANS modeling studies were conducted to find optimal grid design for best compromise between simulation speed and accuracy;
4. Sensitivity studies on slenderness ratio, foil angle/position, and demihull spacing were conducted;
5. Design modifications were made based on sensitivity studies and other structural considerations to arrive at the final design.

5 Potential flow based blending optimization

5.1 Optimization approach

A morphing technique was applied for the parameterization of the hull and foil geometry. Morphing is commonly adopted in image analysis to derive a new image by using a set of base images. In this particular case, the tentative hull and foil shapes are automatically obtained as a weighted sum of the computational grids produced using three base hulls (say, HULL1, HULL2 and HULL3) and foils (FOIL1, FOIL2 and FOIL3). Once the surface grid has been produced for all the given geometries, using the same number of grid panels and an equivalent grid topology, we have a base for the interpolation. Two variables (HU1 and HU2) are used to combine the shape into the interpolation formula. Once the values for HU1 and HU2 are assigned, three coefficients are defined as follows:

$$c_1 = \mathrm{HU1}$$
$$c_2 = (1 - \mathrm{HU1})\mathrm{HU2}$$
$$c_3 = (1 - \mathrm{HU1})(1 - \mathrm{HU2})$$

Using these coefficients, the tentative hull is obtained, point by point, by using the following equation, where x_n is

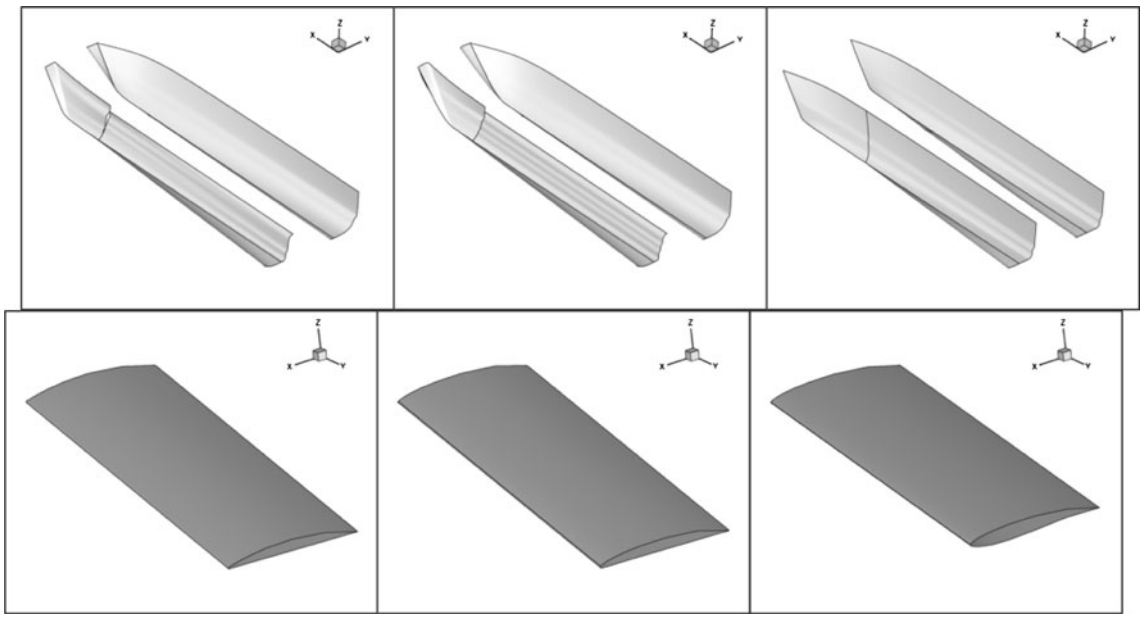

Fig. 3 Perspective views of the three initial shapes of the demihulls and of the central foils adopted as a starting point for the design optimization of RV2. A couple of stern flaps as for SPIRIT are also adopted, being the same for all the given configurations (their shape is not reported here)

the vector of the grid points of the tentative hull in the Cartesian space, and x_1, x_2 and x_3 are the vectors of the grid points of the three base designs in the Cartesian space.

$$x_n = c_1x_1 + c_2x_2 + c_3x_3$$

We recall that, by construction, the following condition holds:

$$c_1 + c_2 + c_3 = 1$$

This approach provides a rationale for mapping the design space onto a unit square, since HU1 and HU2 were varied in between 0 and 1. Necessarily, if HU1 is set to 1 (and hence $c_1 = 1$) all the other coefficients are necessarily zero for any value of HU2. The same procedure is applied to the foil geometry (FOIL1, FOIL2 and FOIL3 are the conventional names for the base designs) and the design variables are FO1 and FO2. Since the demihull spacing was another design variable, the span of the foil was changed accordingly, filling the gap between the hulls.

The three new base designs are reported in Fig 3. The shape of the foils is also reported, showing some differences in the downward angle and in the profile. The three base hulls are combined together by using a morphing technique in order to produce the new hull geometry.

The design variables are represented by the weights for the morphing (two for the hull, two for the foil), while five more variables are also defined, and are reported in Table 1. Objective functions are wave resistance at the two design speeds (Fr = 0.6 and Fr = 1.2) and total resistance at the higher speed (Fr = 1.2). Wave resistance is considered, in a preliminary stage, as representative of associated wave energy, and its minimization is somewhat connected with the reduction of wave wash. Table 1 reports also the design constraints, which involve box constraints on the displacement and some design variables. A large variation of the displacement is allowed in this phase in order to completely understand the effect of a strong variation on this parameter.

Table 1 Description of design variables, constraints and objective functions

Design variables	Box-constraints
Static trim angle (STA)	[−0.3:1.0] deg
Demihull spacing (DSV)	[−2.0:1.0] m
Displacement (DIS)	[72.0:96.0] t
Longitudinal foil position (LFP)	[−1.0:1.0] m
Foil shape parameter 1 (FO1)	–
Foil shape parameter 2 (FO2)	–
Hull shape parameter 1 (HU1)	–
Hull shape parameter 2 (HU2)	–
Stern interceptor height (SIH)	[0:25] mm

5.2 Optimization results

The intensive use of high-fidelity, expensive CFD solver inside an SBD is primarily limited by the computational costs. One way to alleviate this problem is to systematically replace the CFD solver during the optimization phase by using a fast interpolation model (usually called "metamodel") trained on a limited number of expensive simulations,

and then monitoring the discrepancies between the high-fidelity solver and the interpolation model. Here, the space design has been initially populated by 64 different configurations in order to derive the base for the metamodel. In this paper a kriging model [10, 11] was adopted to interpolate the training results. The algorithm here is relatively simple: the optimization process is performed by using the metamodel for the analysis of the ship's performances. Once convergence is obtained, the final shape is validated by the use of the expensive CFD model. The new computation is then added to the training set to obtain an improved metamodel, and the optimization process is repeated until convergence to a final geometry (or the maximum number of iteration) is reached.

To solve the multiobjective problem, the optimization algorithm UNICO [12] has been applied to approximate the Pareto front. It is worthwhile to recall that the Pareto front is the set containing the best trade-off solutions computed by the algorithm, i.e., the so-called non-dominated solutions (i.e., designs that cannot be improved simultaneously under all the criteria by another solution). Indeed, when we are in presence of more than one single objective function, it is very rare to find one single design able to give the optimal value for all the objective functions at the same time. As a consequence, the designer has to deal with a finite set of configurations containing the best compromise solutions, that is, the Pareto set.

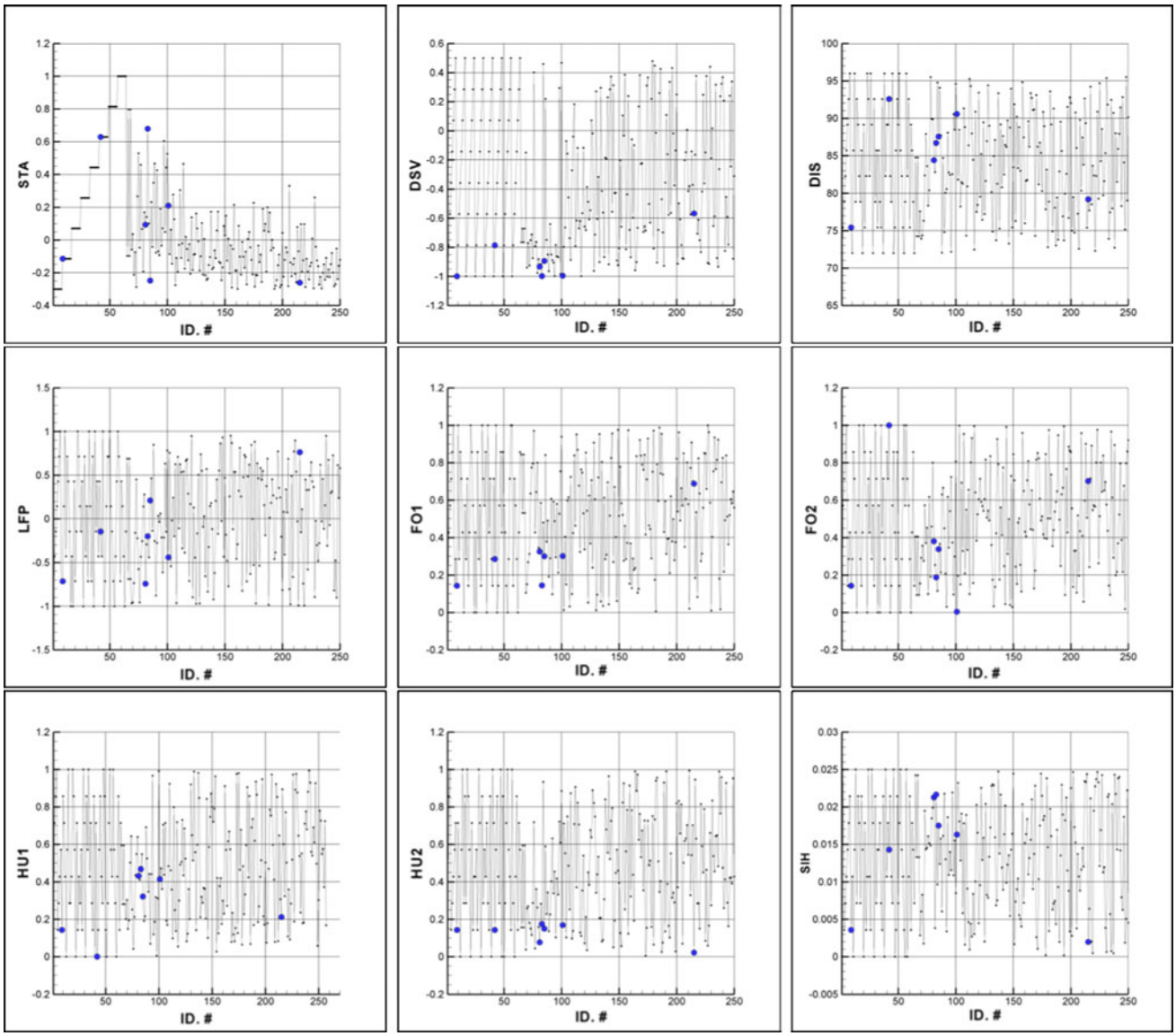

Fig. 4 Values of the design variables as a function of the iteration of the optimization algorithm. The *larger dots* represent the values corresponding to designs that were found to be on the Pareto front

In Fig. 4, the history of the nine design variables values during the entire optimization process is shown. Two different zones are easily noticeable: the first 64 values belong to the training phase. The values of the design variables are assigned according to some user-defined sampling technique (we have adopted here a standard orthogonal array technique), properly selected in order to explore the design space. From configuration number 65 on, the variable values were selected by the UNICO optimizer, looking for Pareto solutions. Indeed, in Fig. 4 we observe that some of the variables show a precise trend, focusing around some value, whereas for other variables the results appear to be more widely spread. This because the Pareto front can be large over the design variable space. The larger dots represent the values corresponding to designs that were found to be on the Pareto front; two Pareto solutions were obtained in the training phase whereas the remaining 5 were found by the optimizer.

After the training phase, which evaluated the 64 different configurations uniformly spread in the design space, the real multiobjective problem was tackled. The optimization algorithm UNICO was applied to identify the Pareto front of the problem. The final results are reported in Fig. 5 and in Tables 2, 3, 4. In Fig. 5, the larger dots are the Pareto optimal solutions, while the smaller circles are all the tested solutions. In Tables 2, 3, 4, the value of the objective functions for the Pareto solutions are reported. The objective functions are nondimensionalized by the value computed for the original HULL1 hull with the FOIL1 foil.

The solution of the multiobjective problem finally gave the following design indications:

5.2.1 *Best designs for a single objective*

A basic indication for the designer is the best hull for each objective function. For F1 (the wave resistance at

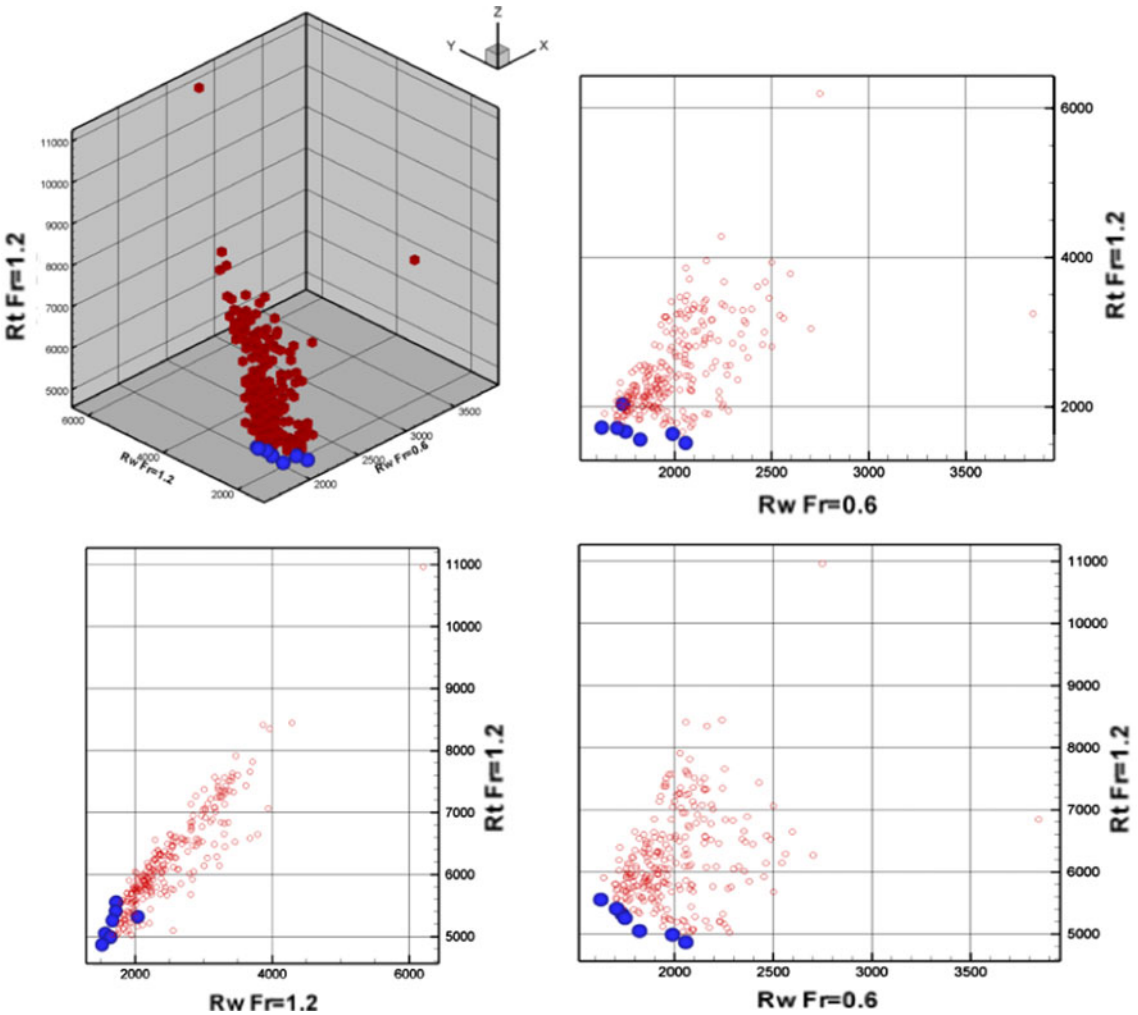

Fig. 5 Different views of the resulting Pareto front: from top to bottom, left to right, a perspective view of the Pareto front, and three different views of the Pareto solutions projected onto the planes at constant F1, F2 and F3 values, respectively

Table 2 Values of the objective functions for the Pareto designs of the optimization problem

Configuration number #	R_W (Fr = 0.6)	R_W (Fr = 1.2)	R_T (Fr = 1.2)
9	0.89981	0.85964	0.89463
42	1.04880	0.82049	0.82520
81	0.92221	0.83529	0.86974
83	1.08427	0.75909	0.80506
85	0.85765	0.86244	0.91858
101	0.96110	0.78224	0.83508
215	0.91504	1.01890	0.87966

Table 3 Values of the hull interpolation coefficients for the Pareto designs of the optimization problem

Configuration number #	C_1	C_2	C_3
9	0.1429	0.1225	0.7347
42	0.0000	0.1429	0.8571
81	0.4324	0.0437	0.5240
83	0.4678	0.0930	0.4392
85	0.3220	0.1018	0.5762
101	0.4147	0.0989	0.4864
215	0.2122	0.0171	0.7707

Table 4 Values of the foil interpolation coefficients for the Pareto designs of the optimization problem

Configuration number #	C_1	C_2	C_3
9	0.1429	0.1225	0.7347
42	0.2857	0.7143	0.0000
81	0.3259	0.2569	0.4172
83	0.1455	0.1611	0.6934
85	0.3015	0.2369	0.4616
101	0.3024	0.0029	0.6948
215	0.6877	0.2192	0.0931

Fr = 0.6) is #85. The best hull for F2 (wave resistance at Fr = 1.2) and for F3 (total resistance at Fr = 1.2) is #83. However #83 is the worst design for the wave resistance at low speed (F1), a clear indication that this design trend is not a good trade off.

5.2.2 Trade-off solution

In an aggregated approach assuming equal importance (i.e. equal weights) among the three objective functions, the best compromise solution appears to be #101, with an aggregated total value of 0.859 (i.e. an improved performance of −14.1%). Table 5 shows the main parametrical differences between the original RV2B and the PF optimized RV3.

Table 5 FAC design parameters

Ship	Displacement	LWL (m)	BWL (demihull) (m)	Spacing (m)	LCG
RV-2B	84MT	24.6	2.32	5.22	10.159
RV3-PF	84MT	25.47	2.7	5.88	9.886

Table 6 Effect of slenderness ratio

Case (m)	DSR	Total resistance (KN)	H (m)
27	9.37	9.321E+01	8.00E−01
29.7	10.38	9.061E+01	7.46E−01

5.3 Verification of potential flow optimization result

The potential flow optimization result (#101, called RV3-PF hereafter) was compared with RV2-B by using URANS for the 37 knot case. For equivalence, the comparisons were made at the same dynamic trim conditions of 0°, which corresponds to LCG = 10.66 m for RV-2B, and LCG = 10.14 m for RV3. The URANS results indicate that RV3-PF has lower total resistance and lower near field wave height by −1 and −3%, respectively. Though the improvement is not as significant as the potential flow calculations, the URANS does confirm an improvement in performance.

6 URANS based systematic sensitivity studies

6.1 Effect of demihull slenderness ratio

The effect of DSR of the ship was studied by increasing the length of the ship by 10% (from 27 to 29.7 m), keeping the displacement constant at 84 metric tons (MT). The foil angle (1.66°) and relative foil position (x/LWL = 0.454 from transom) were kept the same for the comparisons. Also, for one-to-one comparison, the dynamic trim, a function of the LCG, was fixed at 0.1°, and the ship was allowed to heave. The simulations were conducted with the foil attached to the hull.

The results, tabulated in Table 6 show that with an increased slenderness ratio of the demihulls, the maximum near field wave elevation (H) and resistance both decrease. The near field H is defined as the elevation difference between the crest and trough of the first free wave emanating from the ship, which is illustrated in later sections.

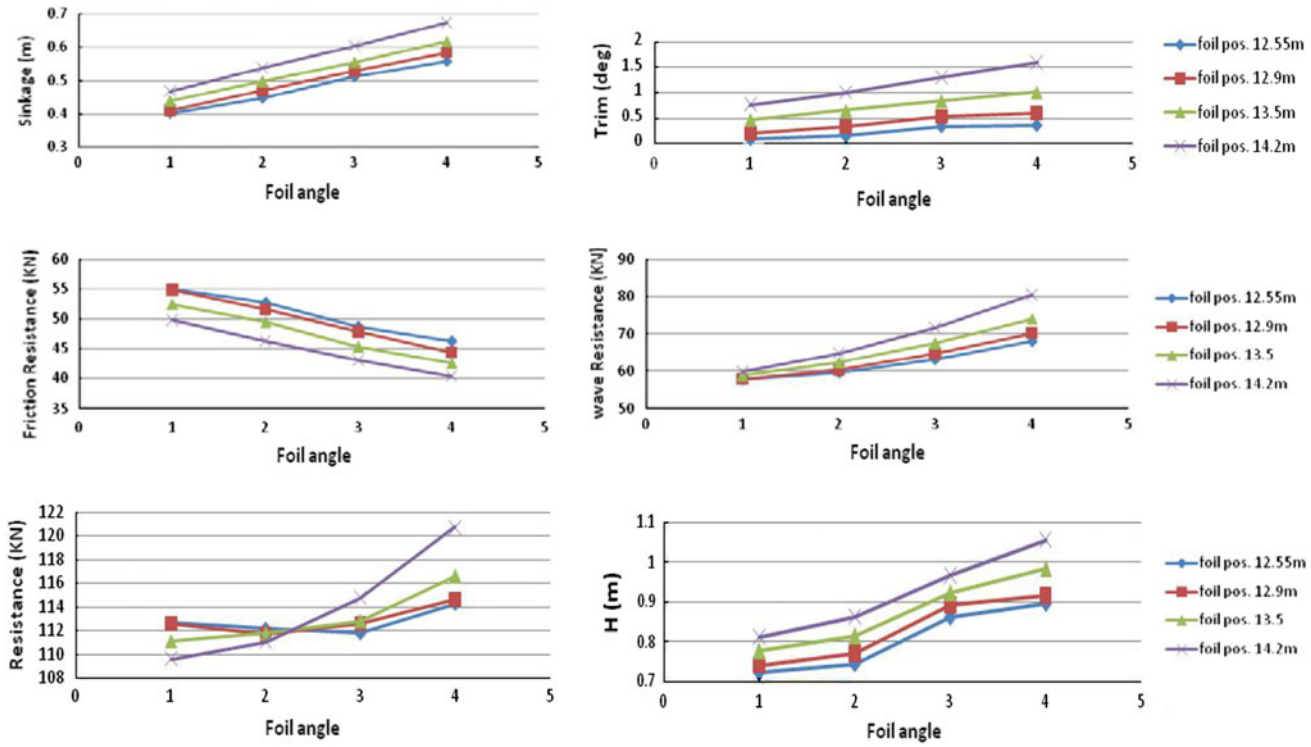

Fig. 6 Foil position/angle studies

6.2 Foil position/angle studies

Position/angle studies on the foil ($c = 1$ m, $t = 0.11$ m) were conducted on the 29.7 m RV3 with foils detached to get the trends. The near field H shows a clear correspondence with the trim angle; H increases with trim. The friction resistance decreases with decrease in wetted surface area, which decreases with trim. However, the wave resistance increases with trim. Combined effect of the two gives the total resistance curve, as seen in Fig. 6. For foil angle >2° there is a sudden increase in gradient for H. Based on these results, configurations with foil angle <2°, and foil position <12.9 m from the transom provide the best compromise between wave height and resistance.

6.3 Effect of demihull spacing

The effect of S_C was explored for different dynamic trim angles obtained by shifting the LCG (Fig. 7). The near field H decreases with increase of spacing as interference effects are lowered. However, there is not much improvement in wave-height by increasing S_C past 6 m; the resistance still shows a decrease with S_C increased past 6 m. For the 6 m spacing, the resistance shows a minimum at LCG = 10.6 m (measured from the stern), corresponding to a trim of 0.85°, as the benefits in frictional resistance are eclipsed by an increase in wave resistance for LCG <10.6 m. For spacing 4, 5, and 7 m, LCG <10.6 m cases were not explored since the trends show unfeasible wave elevation, and also, based on 6 m spacing studies, higher resistance.

6.4 Design modifications based on URANS sensitivity studies

The URANS based sensitivity studies provided general trends which are summarized as follows:

1. Higher DSR reduces both near field H and resistance.
2. Foil angles >2° show a steep increase in gradient for near field H. The additional lift generated at higher angles does not provide significant reduction in resistance.
3. Larger S_C reduces both near field H and resistance. However, the reduction in near field H is negligible past a demihull spacing of 6 m.
4. In general, lowest wave elevations occur at low dynamic trim, at the expense of resistance.

Based on the studies, and additional structural considerations, such as maximum feasible S_C for a particular displacement, the final RV3 (78 MT) design was obtained. The far field wave height spectrum was compared with SPIRIT at a distance of 300 m from the centerline. The far field wave elevation is obtained by using a distribution of Havelock sources which matches the near field RANS wave

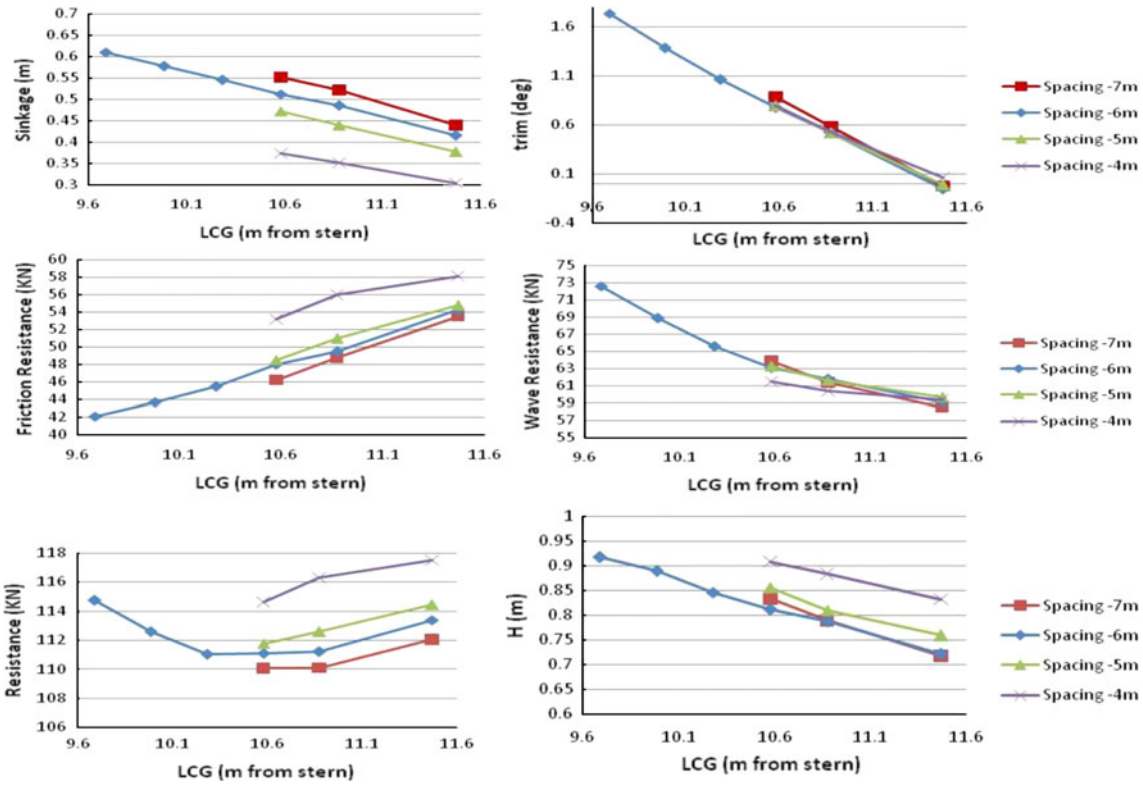

Fig. 7 Demihull spacing studies

elevation as shown in Fig. 8 for the case of SPIRIT at 37 knots. The ship operates in shallow water with sailing line depth of 30 m, and has a supercritical depth Froude number ($Fr_h = 1.1$) at 37 knots. Hence, no steady transverse waves can exist, and the far field ship wake consists solely of divergent waves. The Havelock source code does not take this shallow water effect into account, and hence the computed far field wake was rectified by removing the low frequency transverse waves. Figure 9a shows the computed far field wake at 300 m. The trailing end of the wake train (Fig. 9b) is dominated by the transverse wave component which has a period of 12 s, corresponding to a wavelength of 232 m shown in Fig. 8a; this matches the wave length estimated by the linear theory. The transverse wave was isolated from the wake train by performing a moving average smoothing of the wake train, and correcting the amplitude of the resulting signal to match the trailing end of the wake train. The isolated transverse wave is shown superimposed over the computed wake trains in Fig. 9a, b. Subtracting the transverse wave from the computed wake train results in a wake train composed purely of the divergent waves (Fig. 9c), and the resultant wake is used for obtaining the far field wave height spectra. The far field wake extrapolation procedure used here is detailed in [2].

Figure 10a compares the far field wave height spectra of RV3 with SPIRIT, with the transverse waves removed. The maximum wave height of the divergent waves occurs at period $T = 3$–3.5 s. This corresponds to the wave period of the first free wave. The crest of the first free wave occurs at $y = 10$ m, illustrated by the dashed line in Fig. 8b. The wave elevation at $y = 10$ m is shown in Fig. 10b. Compared to SPIRIT, the maximum wave height for RV3 is reduced. However, the wave heights at periods 4.5–8 s are still greater than the wave height criterion [4]. Hence, a smaller boat was considered by scaling down the RV3. RV3 couldn't be directly scaled down; other structural factors such as width of available propulsion systems and passenger seating had to be factored in. Hence, certain non-dimensional parameters such as DSR and S_C/LWL could not be preserved during the scaling down process. The newly designed scaled down version of RV3, named RV4 (63 MT) showed a significant reduction of wave height over the whole period range and falls below the wave height criterion.

A further reduction in displacement of RV4 to 53 MT was explored by decreasing only the draft and keeping all other parameters the same, with further benefits on both resistance and near field H at 34 knots. But such a decrease in displacement is not possible without a decrease in length, and hence an overall scaling down of the RV4 (63 MT) design was required. However, again, structural design considerations meant that RV4 could not

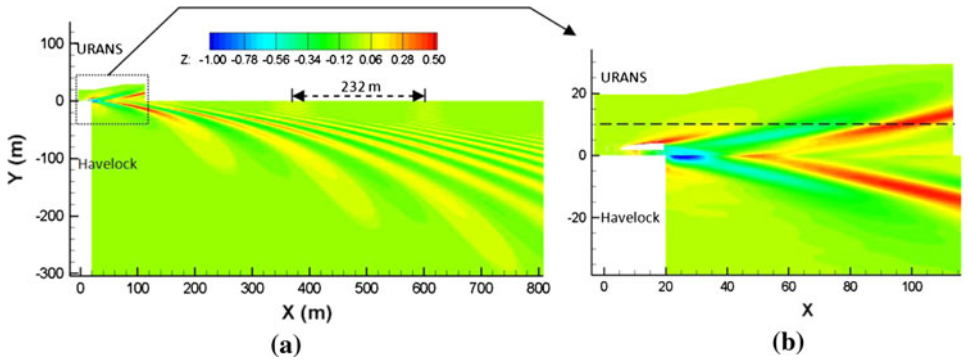

Fig. 8 Far field wake extrapolation using Havelock sources. **a** Far field wake, **b** close-up of near field match

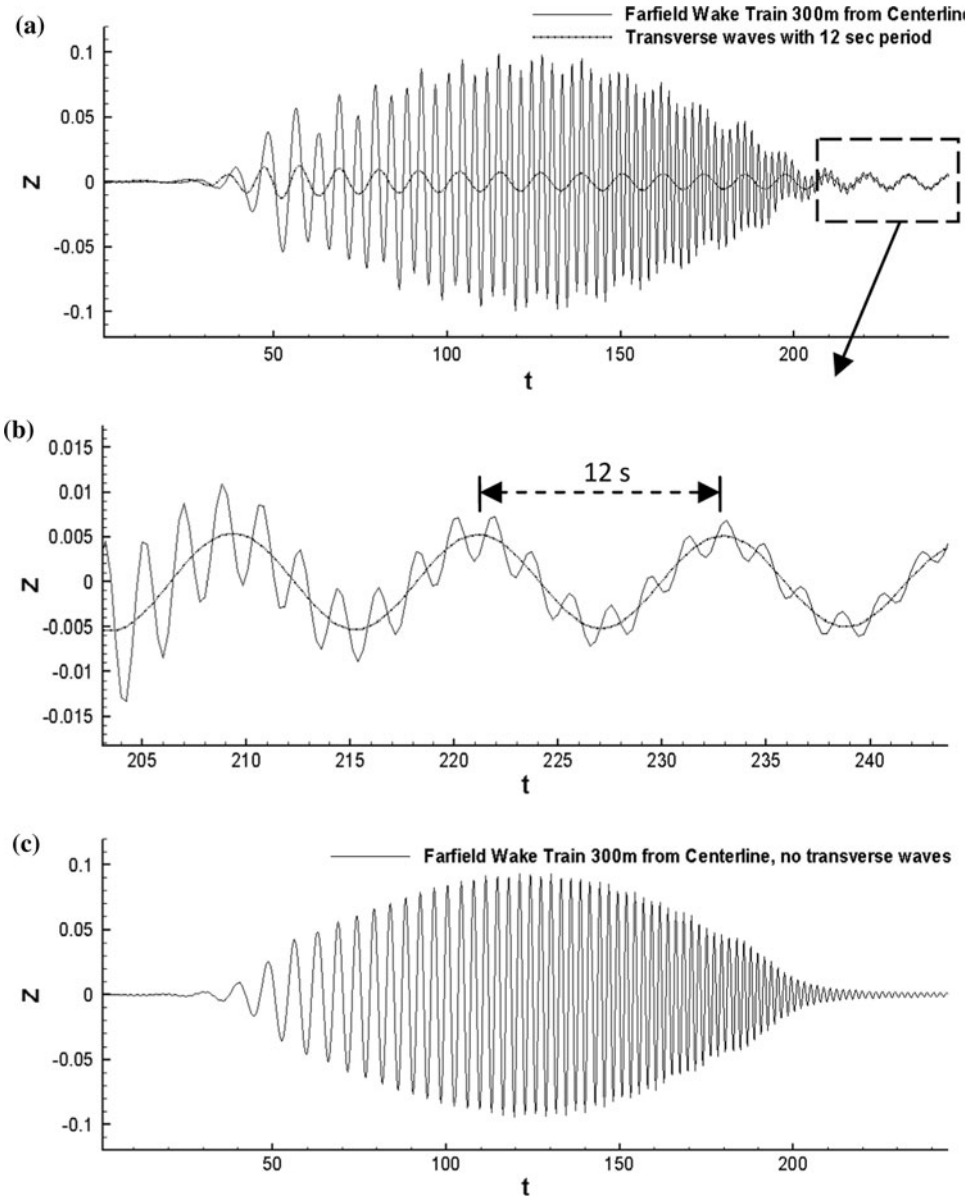

Fig. 9 Far field wake train at 300 m. **a** Computed wake train with transverse wave superimposed, **b** close-up of trailing end of the wake train with dominant transverse wave, **c** wake train with transverse wave removed

be directly scaled down, and hence a newer design RV5 (58 MT) was created. However, RV5 did not show significant benefits compared to RV4 (63MT), since structural considerations led to comparatively lower DSR and S_C/LWL ratios and this affected the performance adversely.

Figure 11 shows the performance comparisons of the designs over the Fr range. The wave energy parameter

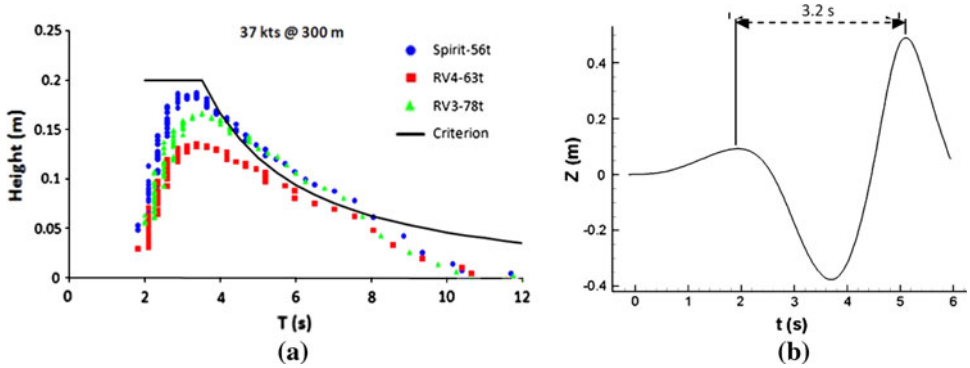

Fig. 10 Wave height, **a** comparison of far field spectra at $y = 300$ m, **b** first free wave at $y = 10$ m for SPIRIT

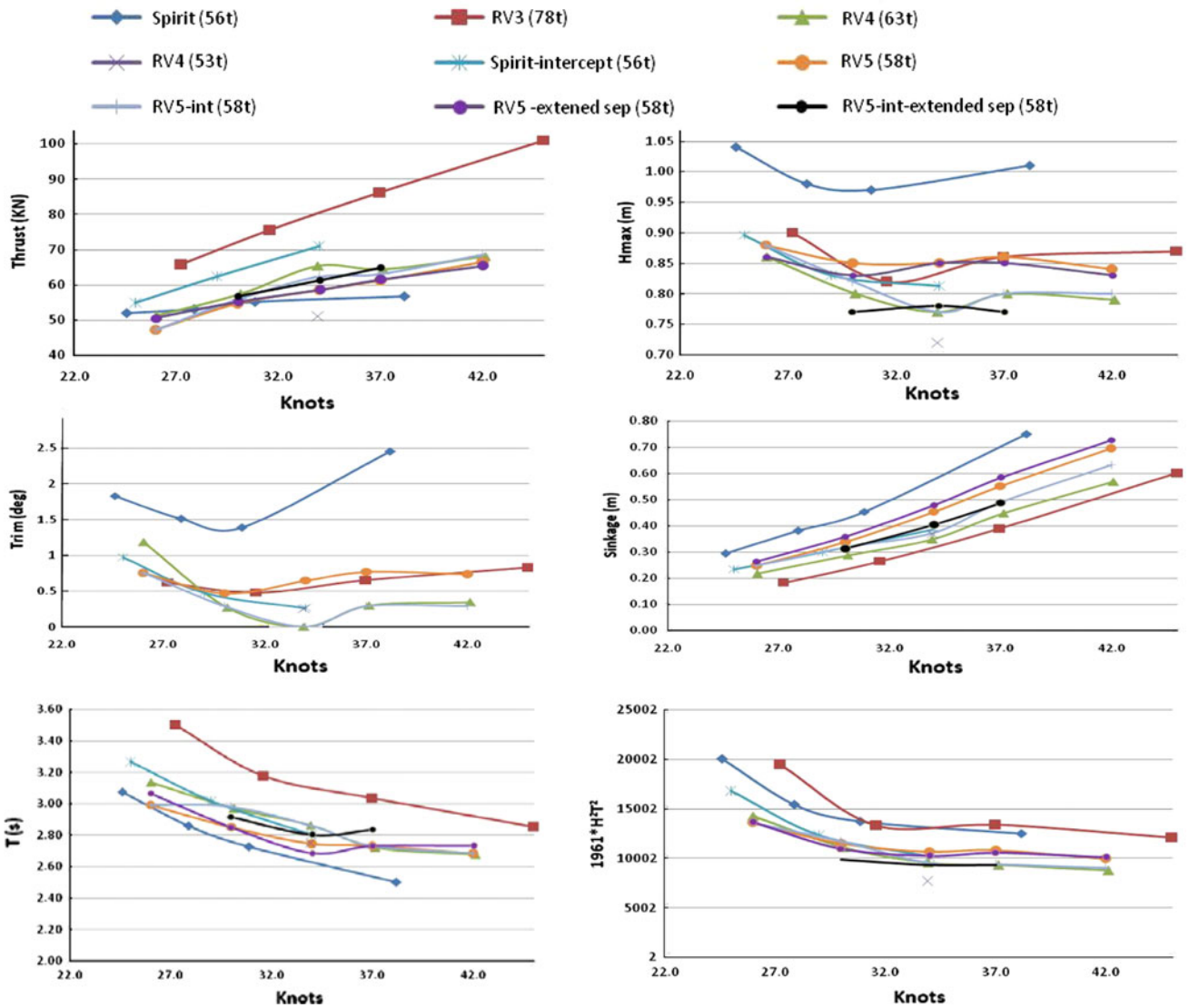

Fig. 11 Performance characteristics of various FAC designs over speed range

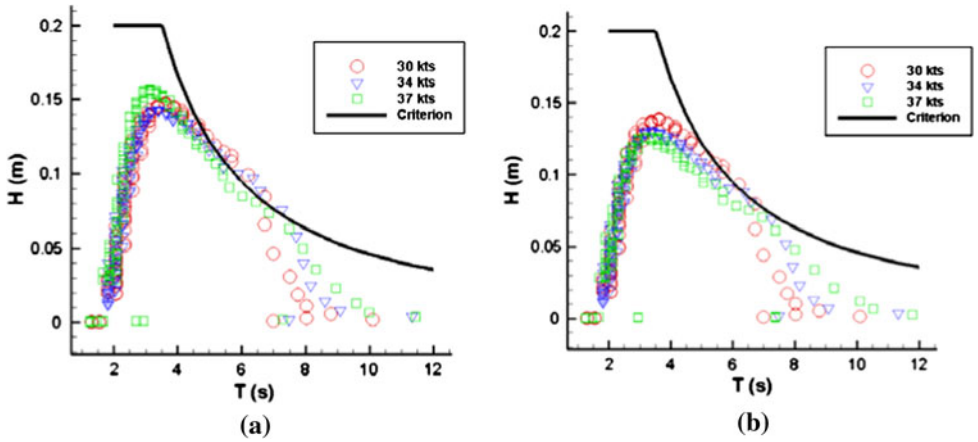

Fig. 12 Far field wave height, **a** without interceptors, **b** with interceptors

Table 7 FAC design evolution

	Spirit	Spirit-int	RV3	RV4-A	RV4-B	RV5	RV5-int-ext
L (hull) m	21.6	21.6	29.7	24.5	24.5	23.5	23.5
B (moulded) m	7.8	7.8	9.8	8.9	8.9	8.3	8.8
Aspect ratio	2.77	2.77	3.03	2.75	2.75	2.83	2.67
Displ MT	56	56	78	63	53	58	58
LWL m	19.721	19.721	28.024	23.096	23.01	22.218	22.218
BWL (demi) m	2.309	2.309	2.699	2.519	2.449	2.464	2.464
BWL (tot) m	4.618	4.618	5.398	5.038	4.898	4.928	4.928
Spacing S_C m	4.2	4.2	5.88	5.33	5.33	4.98	5.48
Draft m	0.992	0.992	0.946	0.99	0.877	1.000	1.000
Block coeff	0.574	0.574	0.531	0.531	0.522	0.515	0.515
Max sect area m^2	0.727	0.727	0.869	0.737	0.871	0.833	0.833
Wetted area m^2	128.48	128.48	170.49	138.49	127.025	132.71	132.71
Demi Slenderness ratio (LWL/BWL)	8.541	8.541	10.383	9.169	9.396	9.017	9.017
Spacing ratio S_C/LWL	0.213	0.213	0.210	0.231	0.232	0.224	0.247
B/T (higher for less drag)	2.328	2.328	2.853	2.544	2.792	2.464	2.464
LWL/Displ$^{0.33}$	6.495	6.495	8.265	7.314	7.719	7.232	7.232
Thrust @ 34 knots KN	56	71	101	65	51	58	57
Wave energy @ 34 knots (near field) J	13100	10173	13350	9544	7690	10670	9124

$E = 1961 \times H^2 \times T^2$ is obtained using the near field H and T. The near field H and T are obtained for all cases at location of the first free wave crest depicted by dashed lines at $y = 10$ m in Fig. 8b. Figure 11 also shows the performance of SPIRIT and RV5 with the effect of the interceptors, i.e., the reduction of trim due to the interceptors was modeled. For spirit-interceptor, simulations used fixed trim obtained from field data for runs with interceptors. Simulations with interceptors were not carried out for the 37 knot case as EFD data were unavailable. For RV5-interceptor, as a reasonable estimate, the trim was set at RV4 (63 MT) trim values which were lower than original RV5 trim values. Reduction of trim to RV4 values also enabled a direct performance comparison with RV4. As noticed before in the sensitivity studies, the reduction of trim leads to lower wave heights and higher resistance. With the interceptors modeled, the RV5-int wave energy is the same as RV4. Interceptors were not modeled for RV4 since the trim values are already very low at design speeds, and interceptors would have negligible effects. It was determined that S_C of RV5 could be increased further by 5% and still satisfy structural constraints. Simulations with this increase in spacing showed decreases in both powering requirements and wave energy compared to RV4 (63 MT). Hence RV5 with interceptors and extended spacing (RV5-int-ext) was chosen as the final design. The interceptor height will be adjustable to be able to fine tune the trim to provide the optimum in terms of wake at different operating speeds and loading conditions. The length (span) will be 1.1 m on each hull and we expect the chord to be in the order of 20 mm to change the trim by 2° at 30 knots. Figure 12 shows the far field wave height spectrum at

$y = 300$ m for the final design with and without interceptors at speeds 30, 34, and 37 knots. Table 7 provides a summary of the design evolution of the FAC.

7 Conclusions

A variable fidelity optimization was carried out for FAC with focus on reducing the wake energy and resistance. The potential flow optimization was carried out by blending three initial hull forms provided by the designer using a global optimization approach. The resulting optimized hull was further refined parametrically by systematic sensitivity studies on DSR, foil angle/position, S_C, and displacement. A far field extrapolation method using Havelock sources developed during the validation phase provided the far field wake height. This process involved close collaboration between the CFD modelers and the ship designers as the constraints on size and shape were dictated by parameters such as cost, passenger seating, and size/shape of available water jet propulsion at different displacements which evolved with the evolution of the design. Simulation results show that the final design being built satisfies the criterion for wake energy with powering requirements within range of available commercial engine and waterjet systems.

The conventional method of predicting resistance and wave data comprises fabricating a physical model and obtaining resistance and wave data by towing the model in a towing tank facility. PF CFD optimization enabled the designers to arrive at a hull and foil geometry which was morphed from three significantly different hull shapes. Such optimization would not be financially viable using conventional towing tank methods. Even though PF provided optimized geometry, it did not provide accurate absolute data in terms of resistance, wave height and wave length. The CFDSHIP-Iowa viscous solver was able to analyze the optimized geometry to obtain data within an accuracy tolerance acceptable for commercial applications. The URANS solver also enabled the designers to further enhance the design through refined optimization of lift components and trim angle, and to find a balanced design which would best meet the original design criteria.

A detailed testing program will be performed on the full-scale ship, which is currently under construction, to validate the results obtained from the URANS solver. Also, the URANS code which was used has been recently updated with improved capabilities for full scale simulations using wall functions [13] and two-phase flow capability for air resistance predictions [14], both of which will be used in future validation simulations with field data from the new full-scale ship.

Acknowledgments Research by IIHR and INSEAN is sponsored by Pacific International Engineering PLLC contract # KT-05-343 under administration of Dr. Philip D. Osborne. The research is being funded under a federal grant program administered by Federal Transportation Administration (FTA-WA-26-7007-2005), designed to support research and investigations of emerging transportation systems. INSEAN is also partially supported by the research project "Programma di Ricerca sulla Sicurezza 2009".

References

1. Peri D, Campana EF, Kandasamy M, Ooi SK, Carrica P, Stern F, Osborne P, Cote J, Macdonald N, Waal ND (2009) Potential flow optimization of a high speed foil-assisted semi-planing catamaran for low wake. 10th International Conference on Fast Sea Transportation, Athens, Greece
2. Kandasamy M, Ooi SK, Carrica P, Stern F, Campana E, Peri D, Osborne P, Cote J, Macdonald N, Waal ND (2009) CFD validation studies for a high-speed foil-assisted semi-planing catamaran. J Marine Sci Technol. doi:10.1007/s00773-011-0120-7
3. Stern F, Carrica P, Kandasamy M, et al (2008) Computational hydrodynamic tools for high-speed sealift: phase II final report. IIHR technical report no. 465. University of Iowa
4. Osborne PD, Hericks DB, Cote JM (2007) Full-scale measurements of high speed passenger ferry performance and wake signature. Proc MTS/IEEE Oceans
5. Balay S, Buschelman K, Gropp W, Kaushik D, Knepley M, Curfman L, Smith B, Zhang H (2002) PETSc user manual, ANL-95/11-Revision 2.1.5, Argonne National Laboratory
6. Noack R (2005) SUGGAR: a general capability for moving body overset grid assembly. AIAA paper 2005-5117, 17th AIAA Computational Fluid Dynamics Conference, Toronto, Ontario, Canada
7. Boger DA, Dreyer JJ (2006) Prediction of hydrodynamic forces and moments for underwater vehicles using overset grids. AIAA paper 2006-1148, 44th AIAA Aerospace Sciences Meeting, Reno, Nevada
8. Bassanini P, Bulgarelli U, Campana EF, Lalli F (1994) The wave resistance problem in a boundary integral formulation, Surv Math Ind 4:151–194
9. Campana EF, Liuzzi G, Lucidi S, Peri D, Piccialli V, Pinto A (2009) New global optimization methods for ship design problems. Optim Eng 10:533–555
10. Matheron G (1963) Principles of geostatistics. Econ Geol 58:1246–1266
11. Peri D (2009) Self-learning metamodels for optimization. Ship Technol Res 56:94–108
12. Peri D, Campana EF (2005) High-fidelity models in global optimization. Lect Notes Comput Sci 3478:112–126
13. Bhushan S, Xing T, Carrica PM, Stern F (2009). Model- and full-scale URANS simulations of athena resistance, powering and seakeeping, and 5415 maneuvering. J Ship Res 53:179–198
14. Huang J, Carrica P, Stern F (2007) Coupled ghost fluid/two-phase level set method for curvilinear body-fitted grids. Int J Numer Meth Fluids 55:867–897